Dynamic Properties of Fly Ash

Rana Chattaraj[1] and Aniruddha Sengupta, A.M.ASCE[2]

Abstract: Due to the ever-increasing demand for electricity, generation of fly ash in large quantities has become a problem throughout the world. The utilization of fly ash in rail and road embankments in earthquake-prone areas requires thorough understanding of its dynamic strength characteristics. A series of resonant column and cyclic triaxial tests have been carried out on fly ash to investigate the influence of various factors on its maximum dynamic shear modulus (G_{max}) and dynamic damping (D_s). Correlations for predicting G_{max} and D_s for fly ash have been proposed. The fly ash is found to be far more liquefiable than sand. The particle-size distribution and low unit weight play a vital role in the determination of cyclic strengths. The dynamic shear damping is found to be very much influenced by the confining pressure and induced strain, but independent of the relative density of the fly ash. The damping of sand is found to be always more than the damping of the fly ash irrespective of the confining pressure. **DOI: 10.1061/(ASCE)MT.1943-5533.0001712.**

Author keywords: Fly ash; Resonant column test; Cyclic triaxial test; Dynamic shear modulus; Damping ratio; Cyclic shear strength.

Introduction

Thermal power plants use more than 260 million t of coal, just in India, as a primary fuel for generating electricity, which accounts for the generation of 112 million tonnes (MT) of coal ash annually (Dhadse et al. 2008). The disposal of ash has already occupied 26,304 ha (65,000 acres) of valuable land just in India alone. To match the growing demand for electricity worldwide due to rapid industrialization and rural electrification, more thermal power plants are coming up with capacity enhancements over existing ones. This is leading to the generation of fly ash at a staggering rate, which is directly responsible for wastage of more valuable land for fly-ash disposal. Recycling this huge amount of fly ash is required for the sustainable development. The fly ash is utilized by the cement industry, in the construction of road embankments, in filling low-lying areas, and by tile and brick industries. In many places, government has made it mandatory to use fly ash in the construction of highway embankments and filling of low-lying areas. Thus fly-ash embankments are being constructed indiscriminately. Proper utilization of fly ash in geotechnical-related construction requires thorough understanding of its strength characteristics subjected to various loading conditions. Numerous researchers suggested different application of fly ash such as utilization of fly ash as bulk fill material, as suggested by DiGioia and Nuzzo (1972), Joshi et al. (1975), and Toth et al. (1988). Stabilization of expansive soil using fly ash was suggested by Ghosh et al. (1973), Vasquez and Alonso (1981), Lo and Wardani (2002), and Erdal (2001). Indraratna and Nutalaya (1991) suggested the usage of pozzolonic fly ash as construction fill.

Permeability and consolidation of compacted fly ash was thoroughly studied by Kaniraj and Gayathri (2004). Ghosh and Subbarao (2007) studied the shear-strength characteristics of Class F fly ash modified with lime and gypsum. Kaniraj and Vasant (2001) performed an experimental program to study the individual and combined effects of randomly oriented fiber inclusion and cement stabilization on the geotechnical characteristics of fly ash–soil mixtures. Compressibility and collapsibility characteristics of a sedimented fly-ash bed were investigated by Madhyannapu et al. (2008). Mohanty and Chugh (2006) conducted a postconstruction performance study on environmental monitoring of a fly-ash-based road subgrade. Effect of time on shear strength and permeability of fly ash was studied by Porbaha et al. (2000). Geotechnical properties of a fly-ash and bottom-ash mixture were studied by Kim et al. (2005) for use in highway embankments. Effect of randomly distributed geofibers on piping behavior of an embankment made with fly ash as fill material was studied by Das et al. (2009). Erdem et al. (2011) conducted an experimental investigation to study the effectiveness of fly ash as a stabilizer for organic soils. Pornkasem et al. (2010) proposed the potential use of fly ash in ground improvement by the cement column technique to reduce the amount portland Type I cement in ground improvement. Ferreira et al. (2003) suggested possible application of municipal solid-waste fly ash at various field such as construction, geotechnical work, agriculture etc. Tuncer et al. (2006) studied the potential use of self-cementing fly ashes as a stabilizer for soft fine-grained soils. Sivakumar and Raja (2014) studied the effect of randomly distributed plastic waste inclusion on the strength and deformation characteristic of fly ash.

Boominathan and Hari (2002) studied the liquefaction strength of fly ash reinforced with randomly distributed geosynthetic fiber/mesh. Liquefaction potential and postliquefaction shear strength of impounded fly ash was investigated by Zand et al. (2009). Jakka et al. (2010) studied the liquefaction behaviors of loose and compacted pond ash. Many of these rail and road fly-ash embankments are located in the earthquake-prone areas and thus their dynamic performance is a major concern. A dynamic analysis requires first determination of the dynamic properties of the embankment materials. However, the review of literature indicates that the strain-dependent dynamic properties (particularly in case of small strain) of fly ash have not received much attention. Hence, this present study seeks to assess the dynamic behavior of fly ash so that its

[1]Research Scholar, Dept. of Civil Engineering, Indian Institute of Technology Kharagpur, Kharagpur, West Bengal 721302, India (corresponding author). E-mail: chattaraj.rana@gmail.com

[2]Professor, Dept. of Civil Engineering, Indian Institute of Technology Kharagpur, Kharagpur, West Bengal 721302, India. E-mail: sengupta@civil.iitkgp.ernet.in

Note. This manuscript was submitted on November 30, 2015; approved on June 14, 2016; published online on August 10, 2016. Discussion period open until January 10, 2017; separate discussions must be submitted for individual papers. This paper is part of the ***Journal of Materials in Civil Engineering***, © ASCE, ISSN 0899-1561.

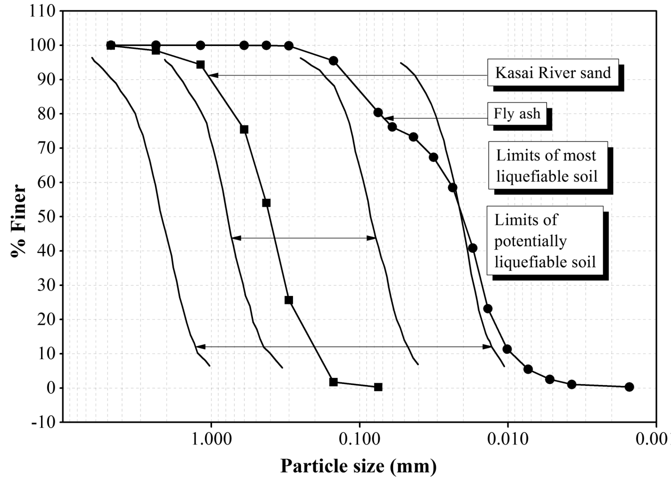

Fig. 1. Particle-size distribution curve of fly ash along with the liquefaction potential boundary

suitability as a construction material in geotechnical engineering problems subjected to dynamic loading may be determined properly. The dynamic properties of the fly ash are compared to those for a locally obtained river sand to understand the differences in behavior between fly ash and sand.

Experimental Investigation

The fly ash utilized in this experimental investigation is collected from a local thermal power plant. The river sand which is used as a reference material is collected from a local river (Kasai River) bed near Kharagpur, India. The grain-size distributions of both the soils are shown in Fig. 1. According to the Unified Soil Classification System [ASTM D2487-11 (ASTM 2011a)] the Kasai River sand is classified as poorly graded sand (SP). It is found that the fly ash consists of mainly silt-sized particles. The index properties of fly ash and Kasai River sand are given in Table 1. The chemical composition of the fly ash as a percentage of dry weight is given in Table 2. According to ASTM Standard [ASTM C618-15 (ASTM 2015)] this fly ash is classified as Class F type fly ash. It may be seen from Fig. 1 that the fly ash consists of mostly silt-sized particles (more than 79% by weight) and for this reason, its plasticity index could not be determined. Accordingly, this fly ash is reported as nonplastic (NP). On the other hand, Kasai River sand contains less than 5% fines. The specific gravity of sand and fly ash are found to be 2.64 and 2.16, respectively, which indicates that fly ash is much lighter than the sand. The ranges of potentially liquefiable soil and most liquefiable soil based on the grain-size distribution as proposed by Tsuchida (Xenaki and Athanasopoulos 2003) are also shown in Fig. 1. It may be seen from the figure that considerable portion of grain-size curve of the fly ash is located within the potentially liquefiable zone where as grain-size curve of the sand is located within the most liquefiable zone. Fig. 2 indicates the compaction characteristics curve of the fly ash and sand utilized in this study. The maximum dry density (MDD) and optimum moisture content (OMC) of the fly ash are found to be 1159.7 kg/m^3 and 32% and for sand 1672 kg/m^3 and 14% respectively. From the vibratory table test, the MDD of the sand is found to be 1.688 g/cc. As the MDD of the sand in vibratory table test is higher than the MDD of the standard Proctor test, the MDD of the sand from the vibratory table test is considered for the test program. It may be seen from the OMC-MDD curves that the moisture density curve for the fly ash is relatively flat, which indicates that the dry density does not change significantly with the variation of the moisture content. Similar findings were also reported by Indraratna and Nutalaya (1991) and Ghosh and Subbarao (2007). They concluded that fly ash can be effectively used as a bulk-fill material as the change in moisture content does not change the field density significantly.

Table 1. Index Properties of Kasai River Sand and Fly Ash

Index property	Kasai River sand	Fly ash
Specific gravity	2.64	2.16
Coarse sand (%)	1.7	0
Medium sand (%)	44.0	0
Fine sand (%)	54	21
Fine content (%)	0.3	79
Maximum void ratio (e_{max})	0.83	2.08
Minimum void ratio (e_{min})	0.56	0.86
D_{10}	0.20	0.0092
D_{30}	0.32	0.013
D_{60}	0.47	0.023
Coefficient of uniformity (C_u)	2.36	2.50
Coefficient of curvature (C_c)	1.08	0.80
UCSC soil classification	—	—

Table 2. Chemical Composition of Fly Ash (Percentage Based on Dry Weight)

Mineral	Percentage
CaO	0.10–3.26
Fe_2O_3	3.56–8.65
Na_2O	8.48
Al_2O_3	34.73–30.67
SiO_2	59.99–60.57

Preparation of the Fly-Ash Samples

All the fly-ash samples are prepared in three layers by using static compaction technique. All the test samples are 70 mm in diameter and 140 mm in length. The height to diameter ratio of the samples is thus kept at 2:1. Depending upon the relative density of the sample to be tested, the required amount of dry fly ash is taken. The required amount of water is then added to the dry fly ash and mixed

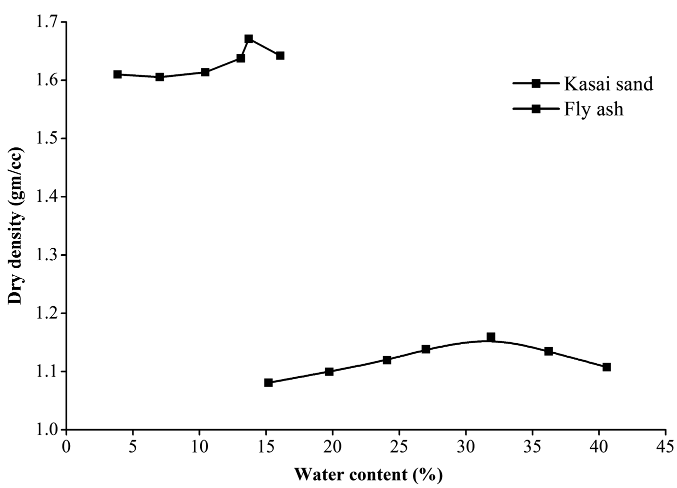

Fig. 2. Compaction curves for fly ash and sand

thoroughly. The prepared fly ash is then poured into a 70 mm diameter mold in three layers. After pouring the fly ash for each layer, static compaction is applied until the layer attained one-third height of the sample to be tested. Before pouring the next layer, the top surface of the previous layer is scarified properly to ensure proper bonding between the consecutive layers. The same process is repeated until the final height of the sample is achieved. The fly-ash sample is then extruded from the mold using a hydraulic jack and used for the tests.

Preparation of the Sand Samples

The sand samples are prepared also prepared in three layers by tamping method as per ASTM D5311-11 (ASTM 2011b). The diameter and height of a sand sample are same as those of a fly-ash sample. A split mold with a 70-mm internal diameter and 140-mm height with an extra detachable collar is utilized for preparing the sand samples. Depending upon the relative density of the sample, sand required for each sample is calculated from the known volume of the mold and separated out in three equal proportions. The sand is then poured into a rubber-membrane-lined split mold using a funnel keeping the drop of height of the soil nearly equal to zero to avoid the segregation of the sand. After pouring each layer, it is compacted by tampering until it occupies one-third of the mold's height. The process is repeated until the full height of the sample is achieved. After completion of this process, a small amount of suction is applied to the sand sample to make it stiff, the split mold is removed, and the triaxial chamber housing the sample is filled with water.

Test Procedure

Resonant Column Test

The resonant column tests on fly ash and sand are carried out on a fixed-free type resonant column device. After mounting the soil sample on the pedestal of the triaxial cell, a torque-producing system that consists of four magnets is attached to the top of the sample. The whole system is then made airtight. A required amount of all-around pressure is applied to the soil sample inside the cell using a computer-controlled air valve system connected to an air compressor. After the application of the all-around pressure, a small amount of current is passed through the coils of the magnetic system at a frequency ranging of 20–200 Hz and at an increment of 5 Hz. This process is done to roughly estimate the natural frequency of the soil sample, and this process is called broad sweeping. This is followed by the fine sweeping, which is done at a range of ± 5 Hz on either side of the roughly estimated natural frequency with an increment of 0.2 Hz to find out the natural frequency of the soil specimen accurately. After this, the voltage in the magnetic coil is increased incrementally and the stated process is repeated for each increment of the voltage. This process is terminated when the strain in the sample exceeds 0.01%. The reference strain, beyond which the shear modulus of the samples is assumed constant, is found to be 0.001% for the sand and 0.002% for the fly ash. For the resonant column tests, sand samples with relative density (RD) of 25, 40, 60, and 80% and fly ash with RD of 70, 80, 90, and 100% are considered. Relative densities are selected such a way so that they can represent the very loose to very dense state. For sand, a 25% relative density considered to be very loose whereas 80% relative density considered to be very dense. Achieving more than 80% relative density for sand in laboratory is very difficult and achieving 100% is impossible. For fly ash, a 70% relative density considered to be very loose and 100% as very dense. Preparing a fly-ash sample with less than 70% relative density is very difficult as it would collapse during extraction from the mold. Such a fly-ash sample would also collapse during the installation of the torque-producing system due to the weight of the system. As in the construction field, 100% compaction is desirable, a 100% relative density is considered as upper limit for the fly ash. Four effective confining pressures of 50, 100, 200, and 400 kPa are considered for both types of soil in resonant column tests. The mass polar moment of inertia of the soil specimen (I_{soil}) is calculated using the following relationship (Kramer 1996) for a fixed-free resonant column:

$$\frac{I_{soil}}{I_{system}} = \beta \tan(\beta) \tag{1}$$

The mass polar moment of inertia of the resonant column drive system (I_{system}) is found out experimentally during installation and calibration of the system. Depending upon the ratio of I_{soil} and I_{system}, the values of β has been found out. In this experimental investigation the ranges of β was found to be 0.332569 to 0.362539. From the known value of β, shear wave velocity V_s is calculated using the following equation (Kramer 1996):

$$V_s = \frac{2\pi l f}{\beta} \tag{2}$$

where f = natural frequency of the soil specimen; and l = length of the soil specimen. Knowing V_s, the shear modulus (G), may be found using the following well-known relationship:

$$G = \rho V_s^2 \tag{3}$$

where ρ = density of the soil specimen.

Cyclic Triaxial Test

After the preparation of the sample within the triaxial cell, an all-around cell pressure is applied to the sample followed by application of a backpressure within the sample with the drainage valves open to saturate the sample. The backpressure is kept between 20 to 25 kPa lower than the cell pressure at all the time. The cell and backpressures are increased simultaneously and the process is terminated when the pore pressure parameter B ($B = \Delta u/\Delta\sigma_c$, where Δu is change in sample pore pressure and $\Delta\sigma_c$ is change in cell pressure) value becomes more than 95%. After the completion of the saturation process, the soil sample is subjected to isotropic consolidation at an effective confining pressure (σ_0) of 100 kPa. After the consolidation process is complete, a cyclic stress ratio (CSR) of varying magnitude is applied to the soil sample until the occurrence of the initial liquefaction. The initial liquefaction is defined as a stage when the ratio of the excess pore-water pressure to the effective confining pressure within the sample becomes 1. To monitor the sample pore-water pressure, cell pressure, axial deformation, and cyclic loading during test, a built-in data acquisition system is utilized. A sinusoidal harmonic loading at a frequency of 1 and 0.1 Hz is applied for the sand and fly ash, respectively. The frequency of 1-Hz loading is commonly used in the study of liquefaction for sand. On the other hand, a 0.1-Hz frequency is chosen for the fly ash. Because of its small grain size, fly ash needs more time to achieve the same pore pressure throughout the sample. The frequencies of 1 Hz for sand and 0.1 Hz for fly ash are also recommended by Jakka et al. (2010).

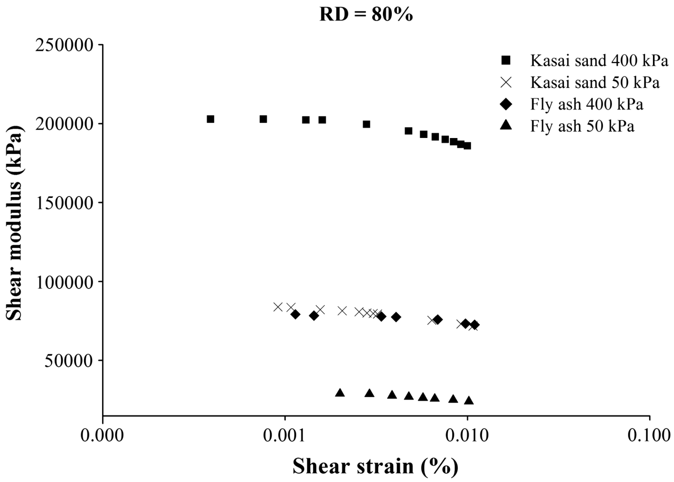

Fig. 3. Variation of shear modulus with strain at different confining pressures for sand and fly ash at RD = 80%

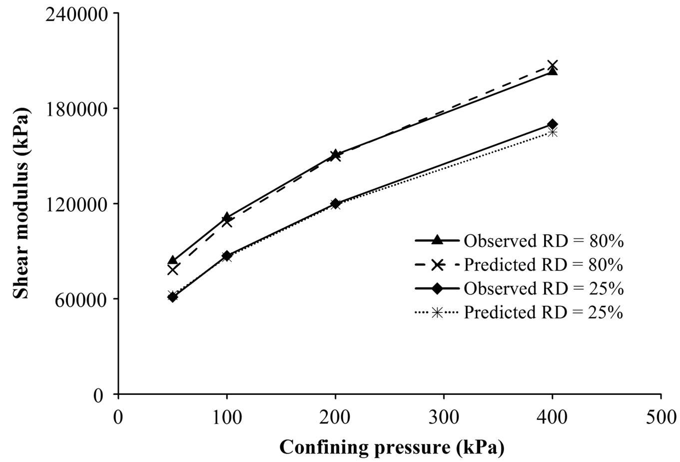

Fig. 4. Predicted and observed G_{max} for sand at RD = 25 and 80%

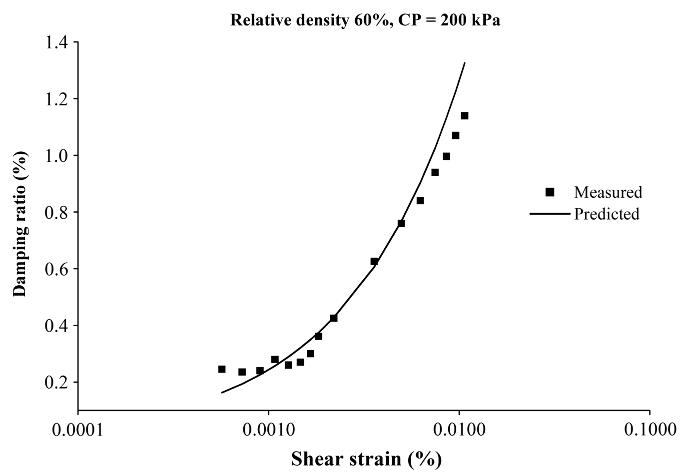

Fig. 5. Predicted and observed damping for sand at RD = 60% and CP = 200 kPa

Results and Discussions

Fig. 3 shows the effect of confining pressure on the variation of shear modulus with strain for Kasai River sand and fly ash at 80% relative density. It is evident from the figure that for a given relative density, the shear modulus of sand and fly ash is directly proportional to the confining pressure. The shear modulus of sand and fly ash increases with the increase in the confining pressure. It is observed that the shear modulus of sand does not change significantly below 0.001% and for that reason, a shear modulus corresponding to 0.001% strain level is treated as the maximum dynamic shear modulus (G_{max}). It is also observed that the shear modulus of sand decreases with strain at all the confining pressure whenever the strain level exceeds 0.001% strain. It can be seen from the Fig. 3 that at 80% RD, the shear modulus of sand at 50 kPa confining pressure is very close to the shear modulus of fly ash at 400 kPa confining pressure.

After conducting a series of resonant column tests on sand, the following correlation for G_{max} and D_s are developed based on the observed experimental data:

$$G_{max} = \frac{611.58 \times (P_a)^{0.532} \times (\sigma_0)^{0.468}}{(0.3 + 0.7e^2)} \tag{4}$$

$$D_s = 41.17 \left(\frac{\sigma_0}{P_a}\right)^{-0.28} (\gamma)^{0.715} \tag{5}$$

where P_a = atmospheric pressure; σ_0 = effective confining pressure; and γ = dynamic shear strain; σ_0 and P_a are in same units and γ and D_s are percentages. There are some standard forms of equations available in the literature for predicting maximum dynamic shear modulus (G_{max}). In this particular case, the form proposed by Hardin (1978) was found suitable. The form of Eqs. (4) and (5) were chosen to make the equation dimensionless and can be used in any system of unit. Fig. 4 compares the data observed during the experimental investigation and the predicted data obtained from Eq. (4) proposed here for relative density of 25 and 80% at different confining pressures. It may be seen from Fig. 4 that the observed G_{max} and the proposed G_{max} are in good agreement. Fig. 5 compares the value of the damping obtained from Eq. (5) with that computed from the experimental data at the confining pressure of 200 kPa for the 60% RD sample. A very close agreement between the two sets of data may be seen from the figure. Fig. 6 compares the value of G_{max} obtains from the proposed Eq. (4) with that of the equation proposed by Hardin (1978). The equation proposed by Hardin (1978) is

$$G_{max} = \frac{625 \times (P_a)^{0.5} \times (\sigma_0)^{0.5}}{(0.3 + 0.7e^2)} \tag{6}$$

It may be seen from Fig. 6 that the predicted data and the data obtain from Hardin's equation are in good agreement.

Effect of Confining Pressure on Shear Modulus of Fly Ash at Small Strain

Variation of shear modulus with strain at different confining pressure for RD of 100% is depicted in Fig. 7. It may be seen from the figure that at constant relative density, the shear modulus degrades with strain. Similar patterns are also observed in sand during dynamic loading. In the case of fly ash, the reference strain is 0.002%. The degradation of shear modulus is often expressed in normalized form. Fig. 8 represents the degradation of shear modulus in fly ash in normalized form. It may be seen from the figure that the rate of degradation of shear modulus is

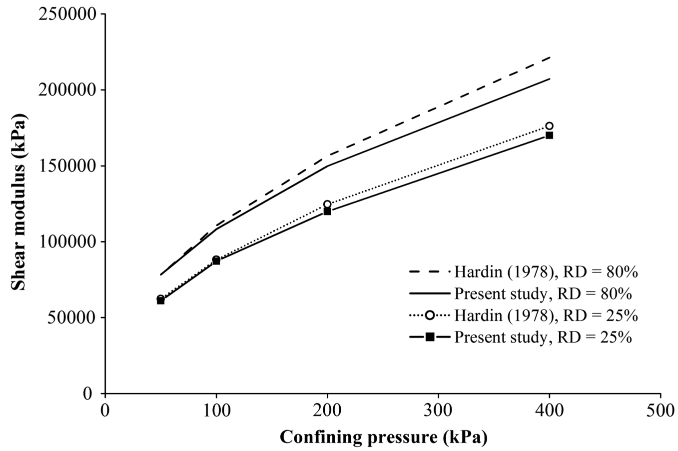

Fig. 6. Comparison between predicted $G_{\max}$ and the $G_{\max}$ obtained from Hardin's equation for sand at RD = 25 and 80%

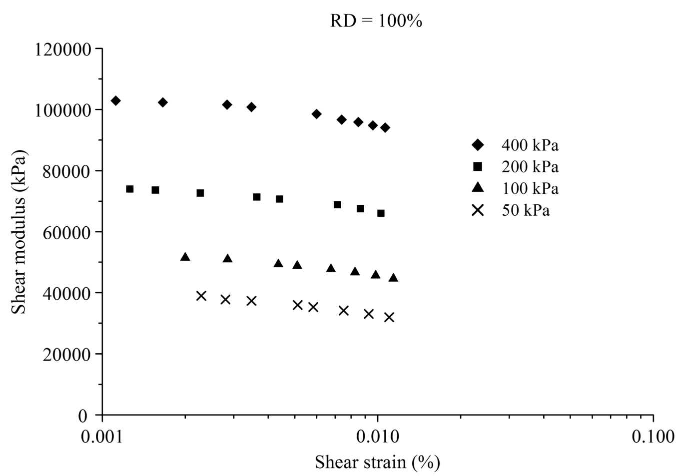

Fig. 7. Effect of confining pressure on the variation of shear modulus with strain for fly ash at RD = 100%

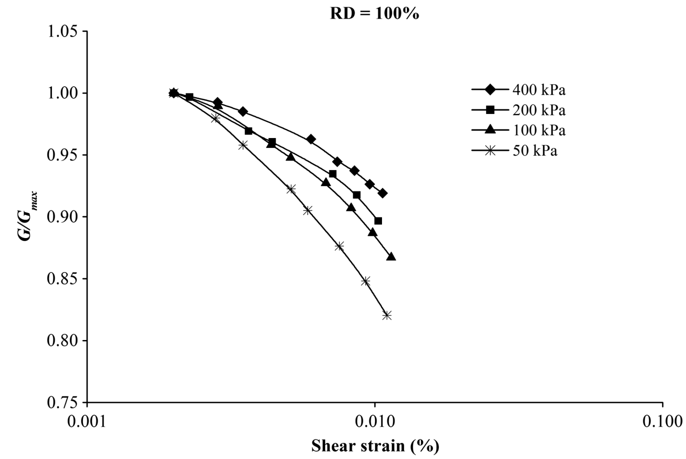

Fig. 8. Modulus reduction curve with strain for fly ash at RD = 100%

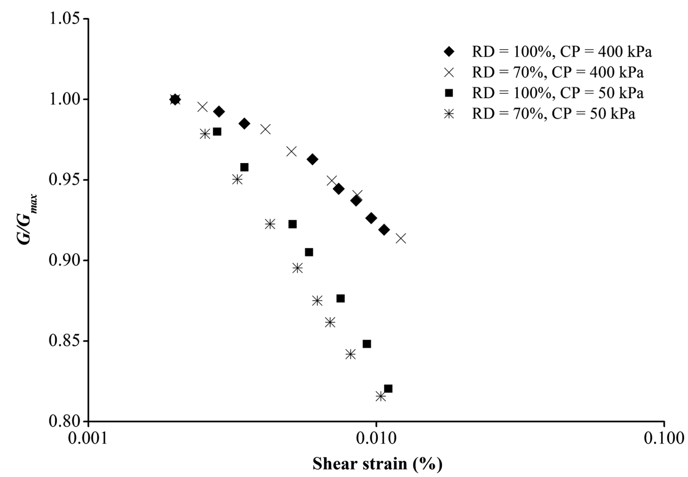

Fig. 9. Effect of relative density on the rate of shear degradation at constant confining pressure for fly ash

inversely proportional to the confining pressure. At 50 kPa confining pressure, the shear modulus degrades by 18% from its peak value at 0.01% strain. However, it is degrades by 8% in case of 400 kPa confining pressure.

Effect of Void Ratio (or Relative Density) on Rate of Shear Degradation at Constant Confining Pressure

Fig. 9 shows the effect of void ratio on the rate of shear degradation with strain. It may be seen from the figure that the effect of void ratio (or relative density) is negligible on the rate of shear degradation at a given confining pressure. At 400 kPa confining pressure, the degradation curves for RD = 70 and 100% almost coincide with each other but at 50 kPa confining pressure, the degradation curves for RD = 70 and 100% disperse by 3% at 0.01% strain.

Correlating $G_{\max}$ with Void Ratio and Effective Confining Pressure for Fly Ash

Based on the regression analysis on the experimentally observed data, the following empirical relationship is developed for the fly ash:

$$G_{\max} = \frac{463.98 \times (P_a)^{0.545} \times (\sigma_0)^{0.455}}{(0.3 + 0.7e^2)} \tag{7}$$

where P_a = atmospheric pressure; and σ_0 = effective confining pressure. The units for P_a and σ_0 are the same. In Eq. (7), whenever void ratio (e) becomes infinite, the $G_{\max}$ becomes zero. This is logical. The described relationship is valid within the confining pressure range of 50–400 kPa.

The measured maximum shear moduli from the experiments are compared with the computed values from proposed relationship and are shown in Fig. 10. It may be seen that the data points are very close to the line of equality, which implies that this proposed equation is very closely approximate the experimentally observed data.

Effect of Confining Pressure on Damping at Small Strain

Fig. 11 shows the effect of confining pressure on damping at constant void ratio. It is evident from the graph that the amplitude of damping is inversely proportional to the confining pressure. It is observed that the amplitude of strain is also an influencing factor. The damping ratio increases with strain irrespective of

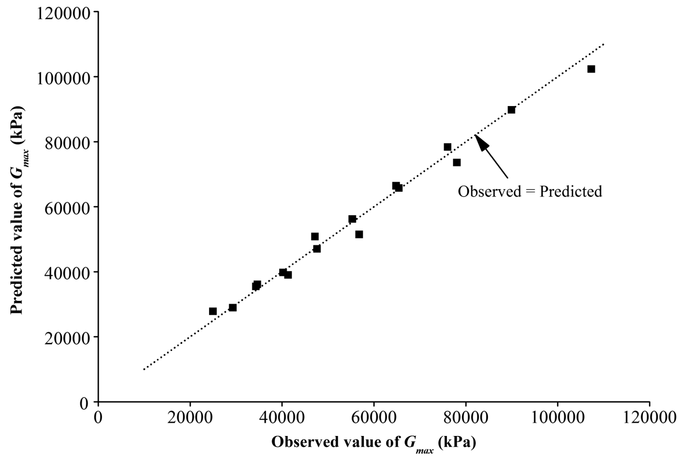

Fig. 10. Evaluation of relationship for maximum shear modulus for fly ash

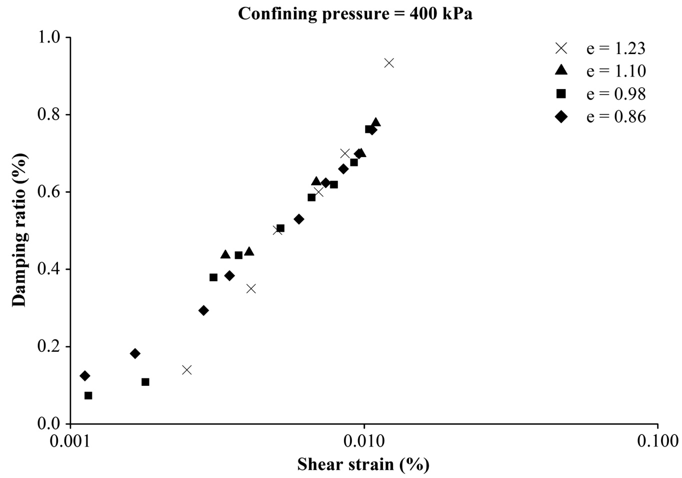

Fig. 12. Effect of void ratio on the variation of damping with strain for fly ash

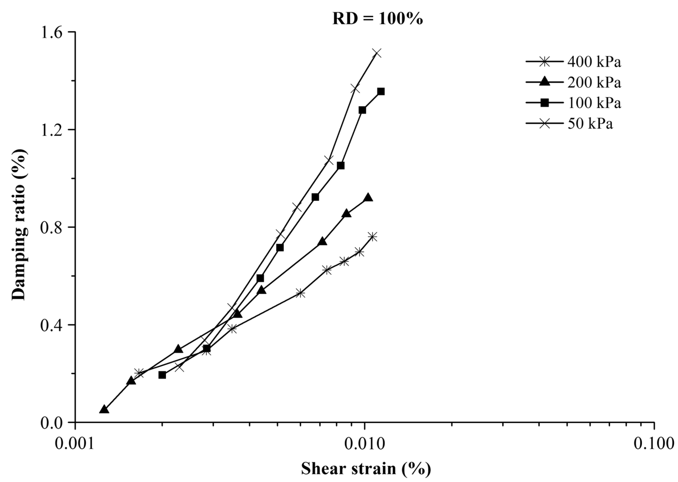

Fig. 11. Effect of confining pressure on the variation of damping with strain for fly ash

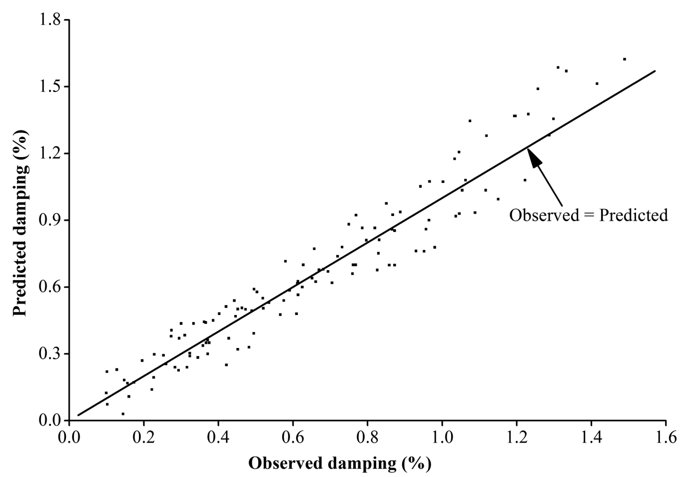

Fig. 13. Evaluation of relationship for dynamic shear damping for fly ash

the confining pressure. The same trend is also observed in the case of sand and reported in literature (Saxena and Reddy 1989; Zhang et al. 2005).

Effect of Void Ratio on Damping at Small Strain

Fig. 12 describes the effect of void ratio on the variation of damping with strain at a constant confining pressure. It may be seen from the figure that the all the data points are within a narrow band, which implies that the damping at constant confining pressure does not depend on void ratio but greatly depends on the amplitude of strain. Similar observations were made by Hardin (1965) and Tatsuoka et al. (1978) in the case of sand. The same effect is also observed for different effective confining pressures.

Correlating Dynamic Shear Damping with Effective Confining Pressure and Strain Percentage

A regression analysis is conducted on the experimentally observed data and the following empirical equation is developed for D_s, which closely approximates the observed data:

$$D_s = 115.65\left(\frac{\sigma_0}{P_a}\right)^{-0.175}(\gamma) \tag{8}$$

where D_s = dynamic shear damping in percentage; P_a = atmospheric pressure; σ_0 = effective confining pressure; and γ = strain in percentage. Units of P_a and σ_0 are same and may be in any system of units as the proposed equation for D_s is dimensionless.

Fig. 13 shows a good agreement between the experimentally observed values and the values calculated based on the proposed relationship for D_s. It may be seen that the data points are in a narrow band and an almost equal number of points are on both sides of the line of equality, which signifies the acceptability of the proposed equation.

Comparison of G_{max} and D_s for Fly Ash and Sand at Small Strain

Fig. 14 represents the G_{max} value of sand and fly ash obtained from the Eqs. (4) and (7) proposed in this study. It is observed that at confining pressures of 50–400 kPa, the G_{max} value of fly ash at the relative densities of 70 and 80% are only 32–38% of the G_{max} value of sand having the same relative densities as fly ash.

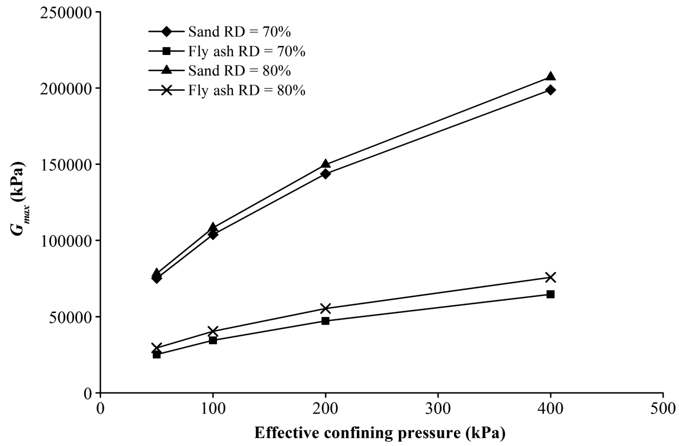

Fig. 14. Comparison of G_{max} for fly ash and sand

Furthermore, the G_{max} value of fly ash at the OMC and MDD is only 51–53% of the G_{max} value of the sand having a relative density of 80%. This value is 64–67% of the sand at a relative density of 25% and at the confining pressure of 50–400 kPa. Low values for dry density and specific gravity of fly ash may be responsible for lower values of G_{max}. Fig. 15 compares the damping behavior of fly ash and sand. As found earlier, the damping values of sand and fly ash do not depend on the relative density but rather depend on the effective confining pressure and amount of strain. This is the reason why the proposed relationships for D_s of sand and fly ash do not have any term related to relative density or void ratio. It may be seen from the figure that the damping of sand is always greater than the damping of fly ash irrespective of the confining pressure. It is observed that at 400 kPa and 0.01% strain, the damping in fly ash is near about 90% of the damping in the sand. At 50 kPa and 0.01% strain, the damping in fly ash is almost 75% of the damping in the sand. This may be attributed to the fact that the stiffness of sand reduces faster than the fly ash as the confining pressure reduces.

Comparison of Cyclic Strength of Fly Ash and Kasai River Sand

Fig. 16 depicts the cyclic strength curve of fly ash at 70% relative density and Kasai River sand at 25% relative density. It may be seen from the graph that the fly ash at 70% relative density is more

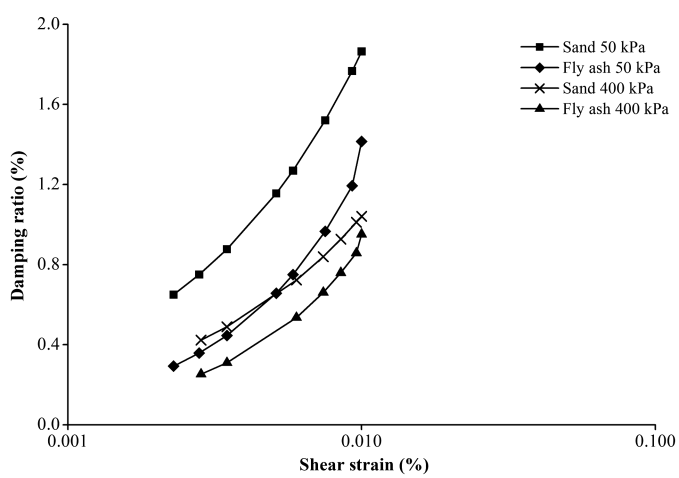

Fig. 15. Comparison of D_s for fly ash and sand

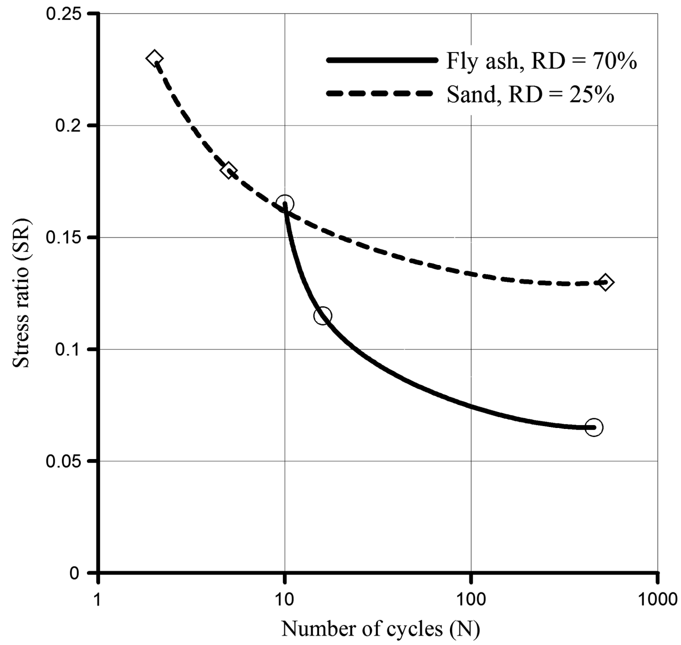

Fig. 16. Cyclic strength curve for fly ash and sand at 70 and 25% relative density

susceptible to liquefaction than the sand at 25% relative density. The cyclic stress ratio required for initial liquefaction at 10, 15, and 20 cycles for fly ash at 70% relative density are 0.165, 0.114, and 0.11, respectively; for sand at 25% relative density, they are 0.17, 0.164, and 0.162, respectively. Though the stress ratio required for initial liquefaction at 10 loading cycles for fly ash and sand at 70 and 25% relative density are almost equal, they vary widely at 15 and 20 cycles of loading. From these findings, it may be concluded that the number of load repetitions drastically reduces the shear strength of the fly ash as compared to sand. This may be due to the low specific gravity and finer particle size of the fly ash. Due to the load repetition, the rate of generation of pore pressure is also higher for fly ash as compared to that in the sand. The finer particles of fly ash reduce the rate of dissipation of excess pore-water pressure due to dynamic loading, which ultimately leads to the reduction in its shear strength. Fig. 17 shows the double-amplitude

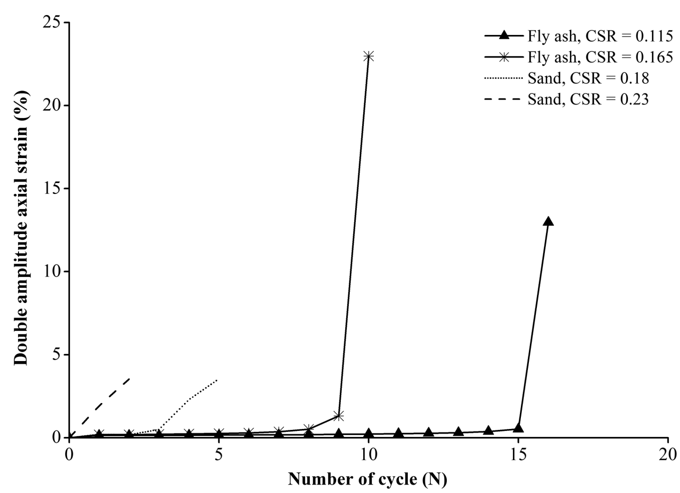

Fig. 17. Variation of double-amplitude axial strain with number of cycles at different CSR values

axial strain at initial liquefaction with number of load cycle for sand and fly ash at 25 and 70% relative density, respectively. The double-amplitude axial strain values for fly ash at 70% relative density at a cyclic stress ratio (CSR) of 0.115 and 0.165 are 12.96 and 22.97%, where as for sand at 25% relative density at CSR of 0.18 and 0.23, the values are 3.53 and 3.62%, respectively. From the figure, it may be concluded that at initial liquefaction, the fly-ash sample deforms more than the sand. The generation of pore-water pressure in cyclic loading conditions leads to faster shear deformation in case of fly ash as compared to sand. Thus due to its low specific gravity and silt-sized particles, fly ash is more susceptible to liquefaction and undergoes larger deformation in the initial liquefaction condition.

Conclusions

The liquefaction potential and dynamic behavior of a river sand and fly ash have been reviewed and compared in this paper. As per Tsuchida's (Xenaki and Athanasopoulos 2003) proposed grain-size distribution ranges for potentially liquefiable soils, the Kasai River sand is supposed to be more susceptible to liquefaction than the fly ash. But dynamic tests on the fly ash and the sand revealed otherwise. The fly ash is found to be far more liquefiable than the river sand. The stress ratio required for initial liquefaction at 15 and 20 cycles of dynamic loading for fly ash at 70% relative density was found to be much lower than those required for the Kasai River sand at 25% relative density. It is observed that along with the particle-size distribution, low specific gravity and/or low unit weight also play a vital role in the determination of the cyclic strength of the soils. It is also observed that the rate of shear deformation during dynamic loading is much higher for fly ash as compared to that for the river sand as the generated pore-water pressures in the fly ash takes a longer time to dissipate due to its finer particle size. Depending upon the confining pressure and void ratio, a new correlation has been proposed for predicting the value of $G_{\max}$ for the fly ash. The proposed correlation has been validated against the laboratory test results. A comparison of $G_{\max}$ value for fly ash has been made with that of the Kasai River sand. It is found that the value of $G_{\max}$ for fly ash is only about 30–40% that of the river sand at the same relative density. It is observed that at a constant relative density, the rate of change of $G/G_{\max}$ is greatly influenced by the confining pressure. But at a constant confining pressure, the rate of change of $G/G_{\max}$ does not significantly depend on the relative density. A new correlation for the damping ratio D_s at various strain levels has been also proposed for fly ash and it is validated against the test results. It is found that the dynamic shear damping is very much influenced by the confining pressure and induced strain, but it does not depend on the relative density of the fly ash. It is observed that the damping of the river sand is always greater than the damping of the fly ash irrespective of the confining pressure. It is observed that at 400 kPa and 0.01% strain, the damping in fly ash is near about 90% of the damping in the sand. At 50 kPa and 0.01% strain, the damping in fly ash is almost 75% of the damping in the sand. This may be attributed to the fact that the stiffness of sand reduces faster than that of the fly ash as the confining pressure reduces. The new correlations for predicting $G_{\max}$ and D_s can be a useful tool for estimating of $G_{\max}$ and D_s for the other fly ash if no test data are available. The presented correlations are strictly valid for a fly ash with the same origin and same grain-size distribution and they need to be validated for other fly ashes.

References

ASTM. (2011a). "Standard practice for classification of soils for engineering purposes (unified soil classification system)." *ASTM D2487-11*, West Conshohocken, PA.

ASTM. (2011b). "Standard test method for load controlled cyclic triaxial strength of soil." *ASTM D5311-11*, West Conshohocken, PA.

ASTM. (2015). "Standard specification for coal fly ash and raw or calcined natural pozzolan for use in concrete." *ASTM C618-15*, West Conshohocken, PA.

Boominathan, A., and Hari, S. (2002). "Liquefaction strength of fly ash reinforced with randomly distributed fibers." *Soil Dyn. Earthquake Eng.*, 22(9-12), 1027–1033.

Das, A., Jayashree, C., and Viswanadham, B. V. S. (2009). "Effect of randomly distributed geofibers on the piping behaviour of embankments constructed with fly ash as a fill material." *Geotext. Geomembr.*, 27(5), 341–349.

Dhadse, S., Kumari, P., and Bhagia, L. J. (2008). "Fly ash characterization, utilization and government initiatives in India: A review." *J. Sci. Ind. Res.*, 67(1), 11–18.

Digioia, A. M., and Nuzzo, W. L. (1972). "Fly ash as structural fill." *J. Energy Eng.*, 98(1), 77–92.

Erdal, C. (2001). "Uses of Class C fly ashes for the stabilization of an expansive soil." *J. Geotech. Geoenviron. Eng.*, 10.1061/(ASCE)1090-0241(2001)127:7(568), 568–573.

Erdem, O., Tuncer, B., Craig, H., and Ahmet, H. (2011). "Stabilization of organic soils with fly ash." *J. Geotech. Geoenviron. Eng.*, 10.1061/(ASCE)GT.1943-5606.0000502, 819–833.

Ferreira, C., Ribeiro, A., and Ottosen, L. (2003). "Possible applications for municipal solid waste fly ash." *J. Hazard. Mater.*, 96(2), 201–216.

Ghosh, A., and Subbarao, C. (2007). "Strength characteristic of Class F fly ash modified with lime and gypsum." *J. Geotech. Geoenviron. Eng.*, 10.1061/(ASCE)1090-0241(2007)133:7(757), 757–766.

Ghosh, R. K., Chadda, L. R., Pant, C. S., and Sharma, R. K. (1973). "Stabilization of alluvial soil with lime and fly ash." *J. Indian Roads Congr.*, 35(2), 489–511.

Hardin, B. O. (1965). "The nature of damping in sands." *J. Soil Mech. Found. Div.*, 91(1), 63–95.

Hardin, B. O. (1978). "The nature of stress-strain behaviour for soils." *Proc., Earthquake Engineering and Soil Dynamics*, Vol. 1, ASCE, Reston, VA, 3–90.

Indraratna, B., and Nutalaya, P. (1991). "Engineering behaviour of a low carbon, pozzolanic fly ash and its potential as a construction fill." *Can. Geotech. J.*, 28(4), 542–555.

Jakka, R. S., Datta, M., and Ramana, G. V. (2010). "Liquefaction behaviour of loose and compacted pond ash." *Soil Dyn. Earthquake Eng.*, 30(7), 580–590.

Joshi, R. C., Duncan, D. M., and McMaster, H. M. (1975). "New and conventional engineering uses of fly ash." *Transp. Eng. J.*, 101(4), 791–806.

Kaniraj, R., and Gayathri, V. (2004). "Permeability and consolidation characteristics of compacted fly ash." *J. Energy Eng.*, 10.1061/(ASCE)0733-9402(2004)130:1(18), 18–43.

Kaniraj, R., and Vasant, G. (2001). "Behavior of cement-stabilized fiber-reinforced fly ash-soil mixtures." *J. Geotech. Geoenviron. Eng.*, 10.1061/(ASCE)1090-0241(2001)127:7(574), 574–584.

Kim, B., Prezzi, M., and Salgado, R. (2005). "Geotechnical properties of fly and bottom ash mixtures for use in highway embankments." *J. Geotech. Geoenviron. Eng.*, 10.1061/(ASCE)1090-0241(2005)131:7(914), 914–924.

Kramer, S. L. (1996). *Geotechnical earthquake engineering*, Prentice-Hall, Englewood Cliffs, NJ, 653.

Lo, S. R., and Wardani, S. P. R. (2002). "Strength and dilatancy of a silt stabilized by a cement and fly ash mixture." *Can. Geotech. J.*, 39(1), 77–89.

Madhyannapu, R. S., Madhav, M. R., Puppala, A. J., and Ghosh, A. (2008). "Compressibility and collapsibility characteristics of sedimented fly ash beds." *J. Mater. Civ. Eng.*, 10.1061/(ASCE)0899-1561(2008)20:6(401), 401–409.

Mohanty, S., and Chugh, Y. (2006). "Postconstruction environmental monitoring of a fly ash-based road subbase." *Pract. Periodicals Struct. Des. Constr.*, 10.1061/(ASCE)1084-0680(2006)11:4(238), 238–246.

Porbaha, A., Pradhan, T. B. S., and Yamane, N. (2000). "Time effect on shear strength and permeability of fly ash." *J. Energy Eng.*, 10.1061/(ASCE)0733-9402(2000)126:1(15), 15–31.

Pornkasem, J., Narongrit, J., Sompote, Y., and Somchai, C. (2010). "Influence of fly ash on unconfined compressive strength of cement-admixed clay at high water content." *J. Mater. Civ. Eng.*, 10.1061/(ASCE)0899-1561(2010)22:1(49), 49–58.

Saxena, S. K., and Reddy, K. R. (1989). "Dynamic moduli and damping ratio for Monterey No. 0 sand by resonant column tests." *Soils Found.*, 29(2), 37–51.

Sivakumar Babu, G. L., and Raja Jaladurgam, M. E. (2014). "Strength and deformation characteristics of fly ash with randomly distributed plastic waste." *J. Mater. Civ. Eng.*, 10.1061/(ASCE)MT.1943-5533.0001014, 04014093.

Tatsuoka, F., Iwasaki, T., and Takagi, Y. (1978). "Hysteretic damping of sands under cyclic loading and its relation to shear modulus." *Soils Found.*, 18(2), 25–40.

Toth, P. S., Chan, H. T., and Cragg, C. B. (1988). "Coal ash as a structural fill with special reference to Ontario experience." *Can. Geotech. J.*, 25(4), 694–704.

Tuncer, B., Hector, A., and Craig, H. (2006). "Stabilizing soft fine grained soils with fly ash." *J. Mater. Civ. Eng.*, 10.1061/(ASCE)0899-1561(2006)18:2(283), 283–294.

Vasquez, E., and Alonso, E. E. (1981). "Fly ash stabilization of decomposed granite." *Proc., 10th Int. Conf. on Soil Mechanics and Foundations Engineering*, Stockholm, Sweden, 391–395.

Xenaki, V. C., and Athanasopoulos, G. A. (2003). "Liquefaction resistance of sand-silt mixture: An experimental investigation of the effect of fines." *Soil Dyn. Earthquake Eng.*, 23(3), 1–12.

Zand, B., Tu, W., Amaya, P. J., Wolfe, W. E., and Butalia, T. S. (2009). "An experimental investigation on liquefaction potential and post-liquefaction shear strength of impounded fly ash." *Fuel*, 88(7), 1160–1166.

Zhang, J., Andrus, D., and Juang, C. (2005). "Normalized shear modulus and material damping ratio relationships." *J. Geotech. Geoenviron. Eng.*, 10.1061/(ASCE)1090-0241(2005)131:4(453), 453–464.